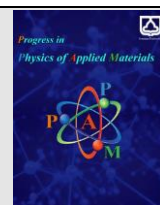




Semnan University

journal homepage: <https://ppam.semnan.ac.ir/>

Effect of Tetraethyl-Orthosilicate, 3-Aminopropyltriethoxysilane and Polyvinylpyrrolidone for synthesis of SiO₂@Ag core-shell nanoparticles prepared by chemical reduction method

N. Jamali, M. M. Bagheri-Mohagheghi*

School of Physics, Damghan University, Damghan, Iran

ARTICLE INFO

Article history:

Received: 6 June 2021

Revised: 26 July 2021

Accepted: 31 July 2021

Keywords:

Ag nano particles
nanocore-metallic shell
sodium borohydride
co-precipitation

ABSTRACT

In this research, silica (SiO₂) and SiO₂@Ag core-shell nanoparticles were synthesized by the co-precipitation method in the presence of ammonia as a reducing agent. First, the effect of different concentrations of tetraethyl orthosilicate (TEOS) as a precursor on the structural and optical properties of silica nanoparticles (SiO₂) was investigated. Then, using this optimized concentration of TEOS, silica nanoparticles with silver shell were prepared by two methods: (a) in the absence and (b) in presence of APTES (3-Aminopropyltriethoxysilane). The properties of SiO₂@Ag core-shell nanoparticles prepared by two methods were compared and the best method was determined. For the synthesis of Ag nanoparticles, silver nitrate (AgNO₃) and sodium borohydride (NaBH₄) as reducing agents were used. To functionalize the surface of silica nanoparticles, 3-Aminopropyl-triethoxysilane (APTES) was added to the AgNO₃ solution with polyvinyl-pyrrolidone (PVP) as a dispersant. The structural properties of silica and silica-silver core-shell nanoparticles were investigated by XRD and TEM. The average size of a silver single crystal in the core shells prepared by the two methods is about 25 nm and 14 nm, respectively. The optical absorption and bandgap were calculated for silica and SiO₂@Ag core-shell nanoparticles. The results indicated that with increasing the concentration of TEOS precursor, the optical absorption of silica nanoparticles increased and their optical band gap reduced from 4.22 eV to 3.55 eV.

1. Introduction

Nano-core shell particles form a special class of nanocomposite materials. They consist of concentric particles in which particles of one material are coated with a thin layer of another material using functionalized procedures [1-6]. recently, efforts to develop core-shell nanoparticles have focused on composite particles with metal nanoshells that have potential applications as catalysts, sensors, support for enhanced Raman scattering, photo-thermal cancer therapy, phototherapy, drug delivery, and colloidal entities with unique optical properties [7-11]. Nanocore-shell materials can be synthesized using any material, like semiconductors, metals, and insulators. Usually, dielectric materials such as silica and polystyrene are used as core because they are highly stable. They are chemically inactive and water-no soluble, therefore, they can be useful in biological applications [12-14].

Metallic nano-shells such as gold and silver can be prepared by a variety of approaches [5, 7, 15-24]. One approach involves a synthesis of core and shell

nanoparticles, separately. Later shell particles can be attached to cores by specialized procedures. In the first method, known as controlled precipitation, the synthesis of shell particles can be carried out in the presence of cores. The core particles act as nuclei and shell material gets condensed on these cores forming nano-shells [25]. Reduction of metal species can be performed using conventional reducing agents such as trisodium citrate or sodium borohydride. In this method, due to the rapid reduction of silver ions, the coverage of the silver shell is low [26]. In the second approach, the surface of the core particles is often modified with bi-functional molecules to enhance the coverage of shell material on their surfaces [27-28]. The surface of core particles such as silica can be modified using bi-functional organic molecules such as APTES (3-Aminopropyltriethoxysilane) [12].

In addition, many composites and core-shell nanostructures have been synthesized from chemical solutions for various applications such as nanocatalyst, bio, and optical sensing, hydrophilic and hydrophobic, and plasmonic resonance by deduction approaches. [29-31].

* Corresponding author. Tel.: +989156202141

E-mail address: bmohagheghi@du.ac.ir

So far, less has been present about the role of parameters and synthesis factors on these nanoparticles. Hence, we have examined the role of these factors such as; Tetraethyl orthosilicate (TEOS) as a precursor, Sodium-borohydride (NaBH_4), and Ammonia (NH_3) as reducing agent, 3-Aminopropyltriethoxysilane (APTES) as activated surface, and Polyvinylpyrrolidone (PVP) as dispersion agent. In addition, providing a simple method with chemical reduction has been one of our goals. In this study, silica (SiO_2) nanoparticles are synthesized by the co-precipitation method. Then, silica nanoparticles with silver shells are prepared by two methods, in the absence and presence of APTES. The optical and structural properties of SiO_2 and SiO_2 @Ag nanoparticles were studied by XRD, TEM, and UV-Vis spectroscopy.

2. Materials and methods

2.1. Materials

Tetraethyl orthosilicate (TEOS) as a precursor, silver nitrate (AgNO_3) as a precursor, Sodium-borohydride (NaBH_4) and Ammonia (NH_3) as reducing agent, 3-Aminopropyltriethoxysilane (APTES) as activated surface, Polyvinylpyrrolidone (PVP) as dispersion, distilled water (H_2O) and Ethanol ($\text{CH}_3\text{CH}_2\text{OH}$) as solvent.

2.2. Synthesis of SiO_2 nanoparticles as core

Silica nanoparticles were synthesized by the co-precipitation method in the presence of ammonia as a reducing agent with various concentrations of tetraethyl orthosilicate (TEOS) as a precursor. Initially, 0.05 M, 0.1 M, 0.15M, and 0.2M of tetraethyl orthosilicate (TEOS) was dissolved in 100 mL of distilled water and 100 mL of ethanol, respectively. Then, 50 mL of ammonia as a reducing agent was added to this solution as a droplet at room temperature. The resulting mixture was centrifuged at 4000 rpm for 15 min, washed with distilled water, and dried in vacuum and a white powder of silica (SiO_2) nanoparticles was obtained (see Fig. 1). The size of these particles was about 150-200 nm. The results showed that the optimal concentration of TEOS is 0.1M.

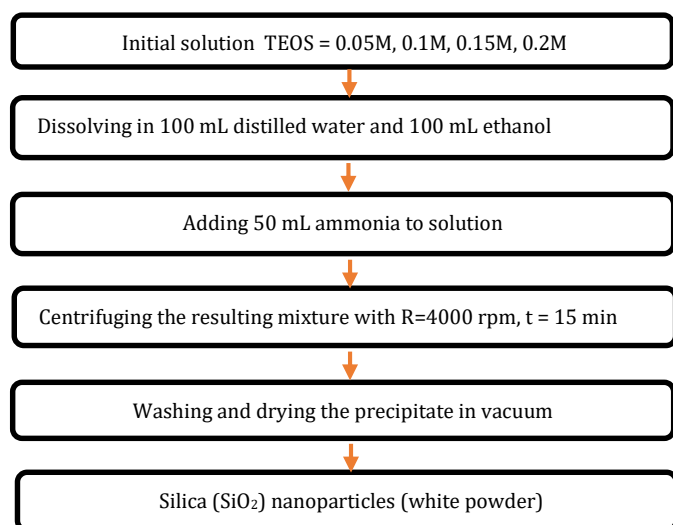


Fig. 1. Flowchart of synthesis of SiO_2 nanoparticles

2.3. Preparation of colloidal solution of silver nanoparticles as shell

A precursor solution of silver nitrate (AgNO_3 , 0.05M) was prepared with 4 g of polyvinylpyrrolidone (PVP) in the presence of ethanol and water as follows: 0.85 g of AgNO_3 was dissolved in 50 mL of distilled water and 50 mL of ethanol. Then, 4 g of PVP was dissolved in 25 mL of distilled water and was added to the solution of silver nitrate and refluxed for two hours at $T=100$ °C. Then, 0.2M of NaBH_4 acting as a reducing agent was added to this solution as a droplet under stirring. Here, the solution was opaque and Ag nanoparticles precipitated.

2.4. Synthesis of SiO_2 @Ag core-shell nanoparticles in absence APTES

In this step, for the synthesis of SiO_2 @Ag core-shell nanoparticles, 25 mg of silica nanoparticles were added to 50 mL of distilled water and were dispersed into it by ultrasonic set. In the next step, 0.05M silver nitrate (AgNO_3) was dissolved in 50mL of distilled water and 50mL of ethanol and added to the above solution. Then, 0.2M aqueous solution of sodium borohydride (NaBH_4) as a reducing agent was added to the resulting mixture dropwise under stirring at room temperature. The resulting mixture was filtered and the precipitate was dried in vacuum.

2.5. Synthesis of SiO_2 @Ag core-shell nanoparticles in presence of APTES

For stability and functionalizing the surface of the silica (SiO_2), we used APTES. Herein, 25 mg of silica nanoparticles were added to 50 mL of distilled water and were dispersed into it by ultrasonic set. Then, 36 mM of APTES was added to it and refluxed for 4 hours at $T=100$ °C. This functionalization process created an amine moiety coating on the outer surface of the silica particles [7]. In the next step, 150 ml of colloidal solution of silver nanoparticles mentioned in section 2.3 was added to the above solution. The resulting solution was refluxed at 110 °C for 4 hours. The resulting mixture was filtered and the precipitate was dried in vacuum.

2.6. Characterization

X-ray powder diffraction (XRD) patterns were measured using a D8 ADVANCE-BRUKER X-ray diffractometer with the CuK_α radiation ($\lambda = 1.54056$ Å) at a scanning rate of 0.04 degrees per second in 2θ ranging from 20°-70°. Transmission electron microscopy (TEM) was performed with an LEO (912 AB) electron microscope. The UV-visible absorbance spectra were recorded at room temperature on a 4802 UNICO UV-Vis Double Beam Spectrophotometer in the range of 300 to 1100 nm. All the samples were diluted with ethanol before taking spectra.

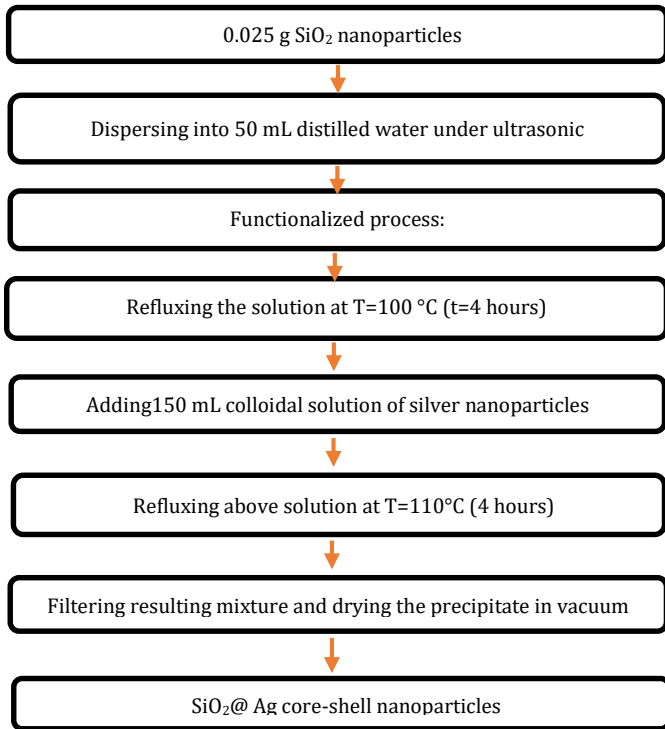


Fig. 2. Flowchart of synthesis of SiO₂/Ag core-shells nanoparticles in presence APTES

3. Results and Discussion

3.1. The XRD analysis: Effect of tetraethyl orthosilicate (TEOS) and APTES

Figure 3 shows the X-ray diffraction (XRD) pattern of the silica nanoparticles with various concentrations of tetraethyl orthosilicate from 0.05 M to 0.2M. As shown, they are noncrystalline, but produce a single broad diffraction peak in the XRD pattern [12], which indicates the amorphous phase of samples. Fig. 4(a) shows the XRD pattern of silica-silver core-shell nanoparticles in absence of APTES. The main diffraction peaks are observed at 2θ= 38.2°, 44.39°, 64.55°, which correspond to the (111), (200),

and (220) planes with fcc phase of silver. The FWHM (β) of the peaks corresponding to (111), (200), and (220) planes are 0.331, 0.429, and 0.435, respectively. According to the well-known Scherrer diffraction formula ($d = k\lambda/\beta\cos\theta$), the average size of a silver single crystal in the composite is about 20-25 nm. Fig. 4(b) shows the XRD pattern of silica-silver core-shell nanoparticles in presence of APTES. The main diffraction peaks are observed at 2θ=38.31°, 44.48°, 64.68°, which correspond to the (111), (200), and (220) planes with fcc phase of silver. The FWHM of the peaks corresponding to (111), (200), and (220) planes are 0.59, 0.598, and 0.728, respectively. The average size of a silver single crystal in the composite is about 12-14 nm. In both methods, results indicate the presence of silver in the samples and the good crystallinity of the resultant nano core shells [7]; however, silica particles have an amorphous phase. The XRD peaks are relatively broad due to the small size of the nanocrystals. In the second method i.e., in presence of APTES, the XRD peaks of samples are broader than the peaks of SiO₂@Ag core-shell nanoparticles in absence of APTES. Therefore, the size of the silver single crystal in the composite is smaller than the size of the silver single crystal in the first method (table 1). This is due to the use of dispersant agent (PVP) in the second method [20]. Table 1 shows the information and results of XRD analysis for SiO₂@Ag core-shells for average crystalline size in two methods of Sherrer and Williamson-Hall using the following equations [21]:

$$d = k\lambda/\beta\cos\theta \quad (\epsilon=0 \text{ and } k= 0.9) \quad (1)$$

$$\beta\cos\theta = 4\epsilon \sin\theta + 0.9 \lambda / d \quad (2)$$

Where ε is lattice strain and d is nanocrystalline size and can be computed from the slope and intercept of the β cosθ and 4sinθ plots, respectively. It can be seen from Table 1 that to consider the ε, the nanocrystalline size was determined more accurately, which is slightly larger than that obtained from the Sherrer equation.

Table 1 Structural information of XRD analysis of SiO₂@Ag core shell nanoparticles

| hkl (Miller index) | 2θ (deg) | Intensity (cps) | Lattice distance (Å) | β(FWHM) (deg) | Crystallite size (nm) By Scherrer | Cos θ | 4 Sin θ | Crystallite size (nm) By Williamson-Hall |
|------------------------------------|----------|-----------------|----------------------|---------------|-----------------------------------|-------|---------|--|
| (a) In the absence of PVP and APS | | | | | | | | ε = - 0.0045 |
| 111 | 38.2 | 3494 | 2.354 | 0.331 | 25.41 | 0.312 | 1.308 | 30.78 |
| 200 | 44.39 | 1195 | 2.039 | 0.429 | 20.01 | 0.397 | 1.511 | 27.52 |
| 220 | 64.55 | 772 | 1.442 | 0.435 | 21.62 | 0.367 | 2.135 | 17.34 |
| (b) In the presence of PVP and APS | | | | | | | | ε = - 0.009 |
| 111 | 38.31 | 1063 | 2.347 | 0.59 | 14.26 | 0.557 | 1.312 | 22.31 |
| 200 | 44.48 | 357 | 2.035 | 0.598 | 14.35 | 0.553 | 1.514 | 15.97 |
| 220 | 64.68 | 316 | 1.439 | 0.728 | 12.92 | 0.615 | 2.140 | 10.05 |

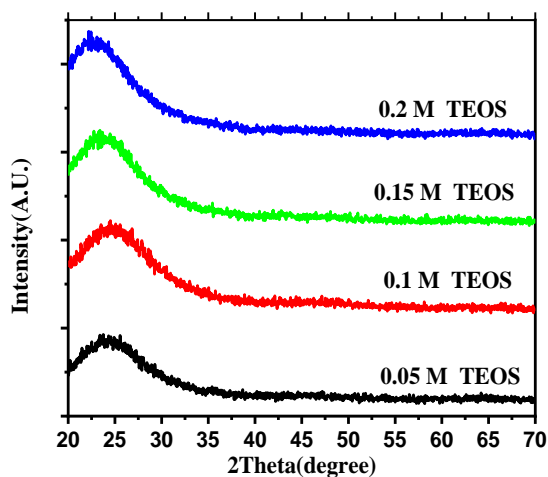


Fig. 3. XRD patterns of silica nanoparticles with various concentrations of TEOS

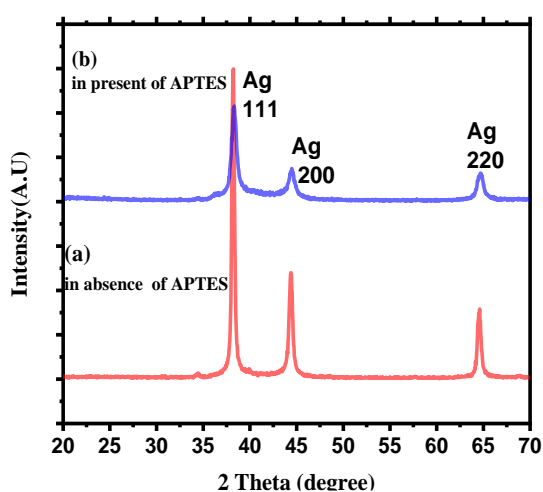


Fig. 4. XRD patterns of silica silver core shell nanoparticles: (a) in absence APTES and (b) in presence of APTES

3.2. Transmission Electron Microscope (TEM) analysis

The TEM images of silica nanoparticles with 0.1M and 0.2M of TEOS are shown in Fig. 5. The TEM images show that, with an increase in the concentration of TEOS, the sizes of silica (SiO_2) nanoparticles are increased [21, 22]. Therefore, the optimal concentration of TEOS is 0.1M in comparison with 0.2M. In this concentration, the shape of silica nanoparticles is a completely spherical form with a uniform size. The size of these nanoparticles is about 150-200 nm. Fig. 6 shows TEM images of SiO_2 @Ag core-shell nanoparticles synthesized (a) in absence of APTES and (b) in presence of APTES. Fig. 6(a) shows that, in absence of APTES, the silver shell coverage is low due to the fast reduction rate of silver ions [26]. In Fig. 6(b), the surface of silica core particles is modified with APTES bi-functional organic molecules to enhance the coverage of shell material on their surfaces [12, 27, 28]. The APTES molecule has an ethoxy group at one end, and an NH group at the other end. APTES forms a covalent bond with silica particles through the OH group and their surface becomes NH-terminated. Now, silver nanoparticles can be attached through the NH group on the silica core [12]. The functionalized process does not change the morphology of a silica particle. It was found that pre-modification of silica with APTES is necessary to generate tailored surface properties, which could immobilize the silver nanoparticles on the surface of silica particles. Silver nanoparticles with small size are attached to the APTES functionalized silica surface; due to the aminophilic nature of silver particles. These small colloidal particles matched to lone pairs of the terminal amine groups, which stabilize(s) the silver nanoparticles on the surface of silica [7]. Table 2 shows the structural properties of core/shell nanoparticles for metallic and semiconductor oxides with various applications.

Table 2
Silver (Ag) containing multinary core@shell nanostructures

| Nature | Core/shell composition | Synthetic strategy | Size (nm) | Application | Reference |
|------------------------|------------------------|----------------------|-----------|----------------------------------|-----------|
| Binary Nanostructures | Ag/Au | Seed-mediated growth | 10.7 | Antimicrobial activity | [32] |
| Ternary Nanostructures | Ag/Au/Pd | Seed-mediated growth | 13.6 | Catalysis (dye degradation) | [33] |
| Ternary Nanostructures | Au/Ag/Pd | Co-reduction | < 100 | plasmonic catalysis | [34] |
| Core/shell | SiO_2 /Au | Co-reduction | < 200 | water quality monitoring | [35] |
| Core/shell | SiO_2 /Cu | Co-reduction | 75-100 | surface plasmonic resonance | [36] |
| Core/shell | SiO_2 /Ag | Co-reduction | 80-100 | Photothermal and bioimaging | [37] |
| Core/shell | SiO_2 /Ag | Co-reduction | < 100 | nonlinear optical | [38] |
| Core/shell | SiO_2 /Ag | Co-reduction | < 150 | Optical shift and photocatalysis | this work |

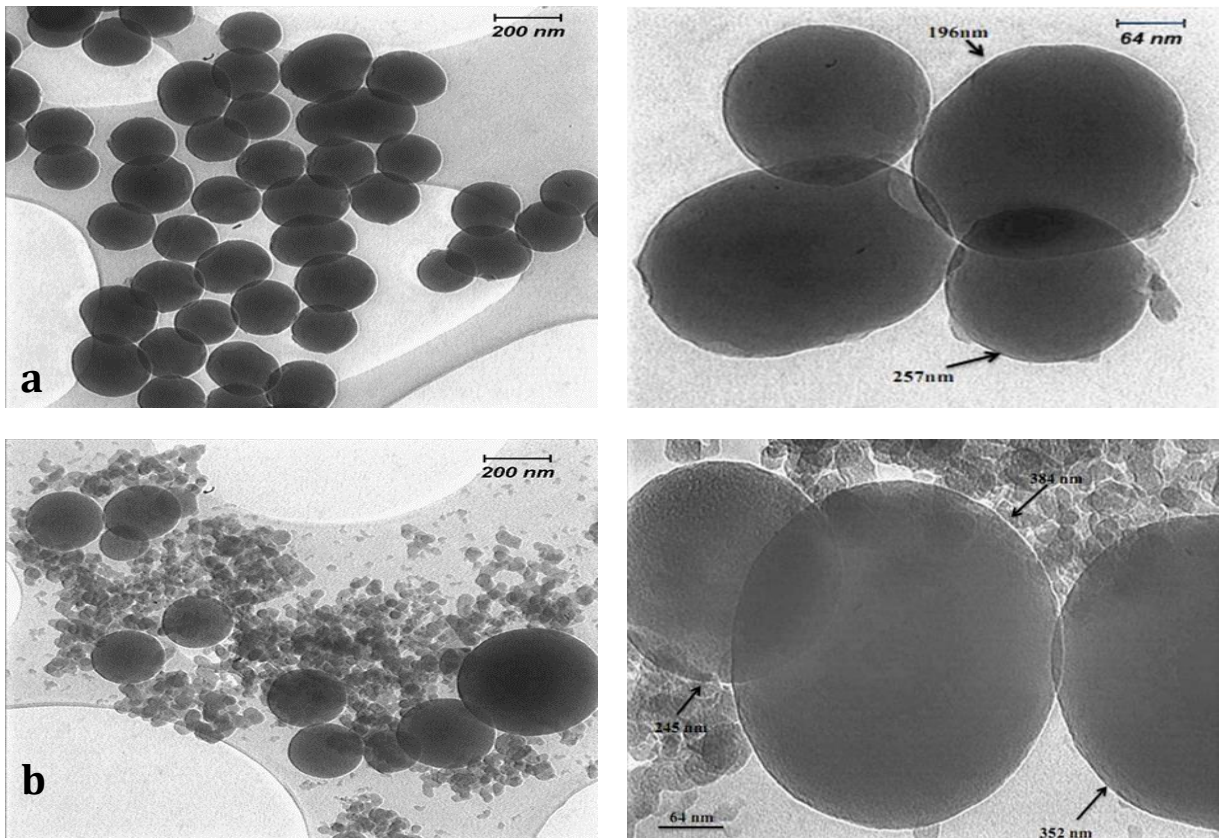


Fig. 5. TEM images of silica nanoparticles with TEOS concentrations: (a) 0.1 and (b) 0.2 M

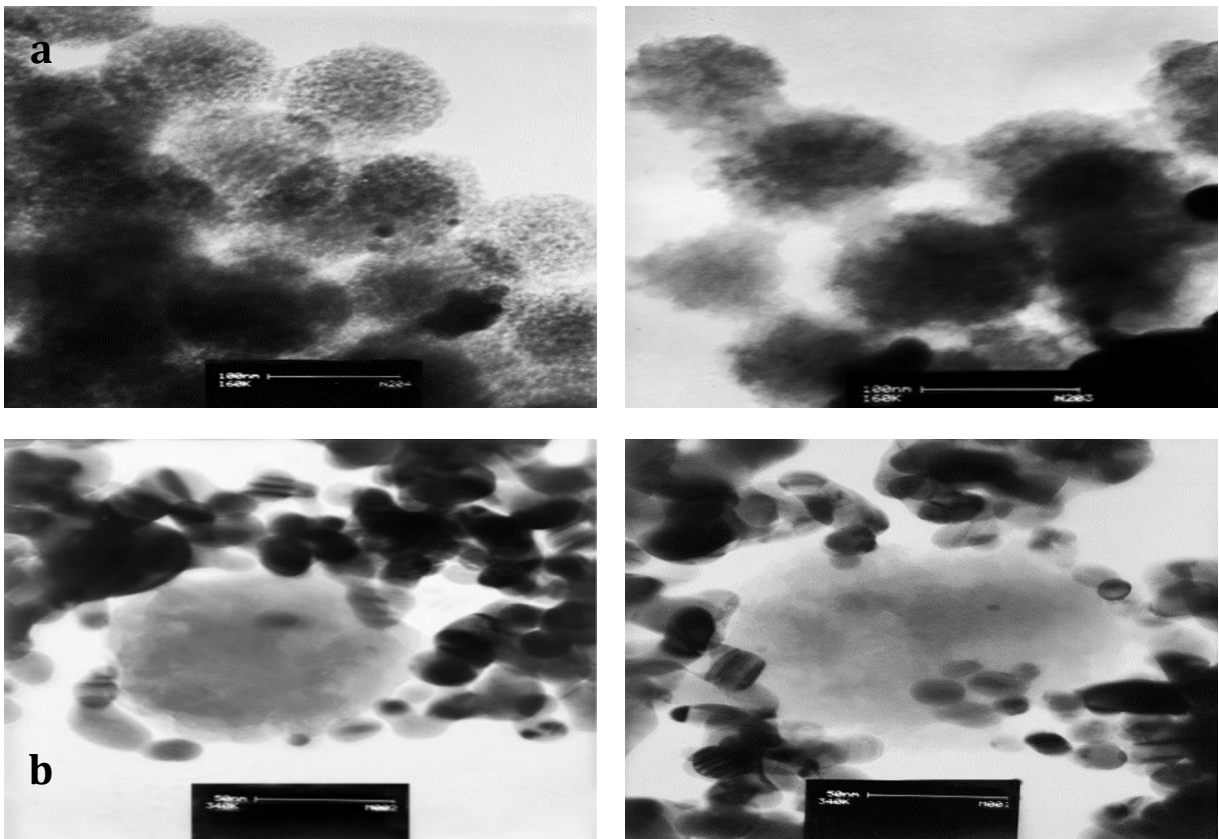


Fig. 6. TEM images of silica silver core shell nanoparticles: (a) in absence of APTES and (b) in presence of APTES

3.3. Determination of band gap energy of SiO₂@Ag core shell by UV-Vis spectroscopy

UV-Visible spectroscopy was employed for further qualitative characterization of the optical properties of the samples. The optical absorbance of silica nanoparticles with various concentrations of TEOS is shown in Fig. 7. As seen, it can be noticed that with increasing the concentration of TEOS, the optical absorbance of nanoparticles has been increased and their optical band gap (Fig. 8) is decreased from 4.22 eV to 3.55 eV, because with increasing the concentration of TEOS, the size of silica nanoparticles is increased [7, 12, 23-25], and the dielectric function of silica is constant in the wavelength range of 300-1100nm [7, 12, 28].

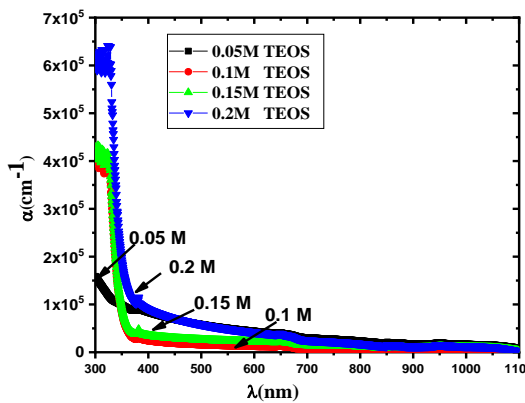


Fig. 7. Optical absorbance diagrams of silica nanoparticles with various concentrations of TEOS

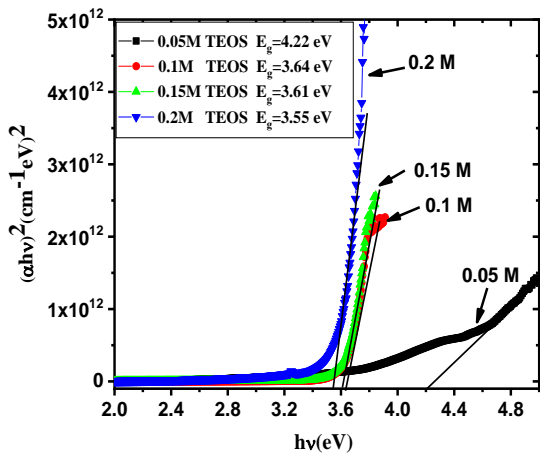


Fig. 8. Bandgap diagrams of silica nanoparticles with various concentrations of TEOS

However, in absence of APTES, there is a weak broad peak at about 400 nm (Figure 9a) after deposition of discrete silver nanoparticles. This is due to surface plasmon resonance excitations from the metal nanoparticles [25]. As shown in Figure 9b, in presence of APTES, there is a broad peak at about 400 nm due to surface plasmon resonance from the single Ag nanoparticles [26, 27] and a new absorption peak at a longer wavelength (about 600 nm) appeared, which may be ascribed to the collective absorption behavior of Ag particles on the core surface [27, 28]. As indicated, the formation and growth of silver nano-shells in presence of APTES is better than in absence of APTES [7]. This is because APTES enhances the coverage of

silver shells on the surface of silica core particles [12, 27-28]. APTES forms a covalent bond with silica particles through the OH group and their surface becomes NH-terminated. Then, silver nanoparticles attached through the NH group on the silica core [12]. Recently, various nanostructures and nanocomposites have been prepared by hydrothermal and hammer reduction methods for magnetic and photocatalytic applications [29-31].

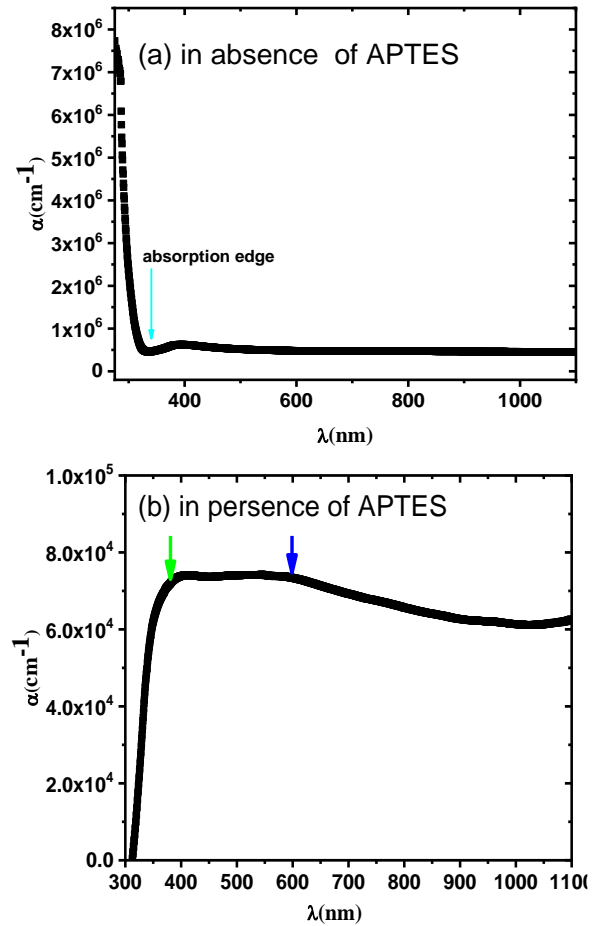


Fig. 9. Optical absorbance diagrams of silica silver core shell nanoparticles: (a) in absence of APTES and (b) in presence of APTES

4. Conclusion

In summary, silica nanoparticles are synthesized by the co-precipitation method. Then, silica nanoparticles with silver shells are prepared by two methods, (a) in absence of APTES and (b) in presence of APTES. In these methods, the results show the presence of silver in the samples and the good crystallinity of the resultant nano core shells; however, silica particles were amorphous. The XRD peaks are relatively broad due to the small size of the nanocrystals. In the second method due to the use of dispersant agent (PVP), the XRD peaks of samples are broader than the peaks of SiO₂@Ag core-shell nanoparticles in the first method. Therefore, the size of the silver single crystal in the composite is smaller than the size of the silver single crystal in the first method. By increasing the concentration of TEOS, the sizes of silica nanoparticles are increased. Therefore, the optimal concentration of TEOS is 0.1M in contrast with 0.2M. In this concentration,

the shape of silica nanoparticles is a completely spherical form with a uniform size. In absence of APTES, the silver shell coverage is low due to too the fast reduction rate of silver ions. Therefore, the surface of silica core particles is modified with APTES bi-functional organic molecule to enhance coverage of silver shell on their surfaces. The size of silica nanoparticles increases with increasing the concentration of TEOS; therefore, the optical absorbance of silica nanoparticles is increased and their optical band gap was decreased from 4.22 eV to 3.55 eV. However, in absence of APTES, there is a weak broad peak at about 400 nm due to surface plasmon resonance excitations from the metal nanoparticles after deposition of discrete silver nanoparticles. In presence of APTES, there is a broad peak at about 400 nm due to surface plasmon resonance from the single Ag nanoparticles and a new absorption peak at a longer wavelength (about 600 nm) appeared, which may be ascribed to the collective absorption behavior of Ag particles on the core surface. This is because APTES enhances the coverage of silver shell on the surface of silica core particles. Silver nanoparticles attached through the NH group on the silica core.

References

- [1] L.M. Liz-Marzan, M.A. Correa-Duarte, I. Pastoriza-Santos, P. Mulvaney, T. Ung, M. Giersig, N.A. Kotov, In Hand Book of Surfaces and Interfaces of Materials (ed. Nalwa, H. S.), Nanostructured Materials, Micelles and Colloids, Ch. 5, 3 (2001) 189.
- [2] R. Davies, G.A. Schurr, P. Meenam, R.D. Nelson, H.E. Bergna, C. A. S. Brevett, R. H. Goldbaum, Engineered particle surfaces. *Adv. Mater.* 10 (1998) 1264-1270.
- [3] A. C. Templeton, W. P. Wuelfing, R. W. Murray, *Acc. Chem. Res.* 33 (2000) 27-36.
- [4] F. Caruso, Nanoengineering of particle surfaces, *Adv. Mater.* 13 (2001) 11-22.
- [5] Y. Xia, B. Gates, Y. Yin, Y. Lu, Monodispersed colloidal spheres: old materials with new applications. *Adv. Mater.* 12 (2000) 693-713.
- [6] S.J. Oldenburg, R.D. Averitt, S.L. Westcott, N. Halas, Nanoengineering of optical resonances, *J. Chem. Phys. Lett.* 288 (1998) 243-247.
- [7] Z.J. Jiang, C.J. Liu, Seed-mediated growth technique for the preparation of a silver nanoshell on a silica sphere, *Phys. Chem. B.* 107 (2003) 12411-12415.
- [8] D.I. Gittins, A.S. Sussha R. Wannemacher, Dense Nanoparticulate Thin Films via Gold Nanoparticle Self-Assembly, *Adv. Mater.* 14 (2002) 508-512.
- [9] S.J. Oldenburg, J. B. Jackson, S. L. Westcott, N.J. Halas, Infrared extinction properties of gold nanoshells, *Appl. Phys. Lett.* 75 (1999) 2897-2899.
- [10] T. Pham, J.B. Jackson, N.J. Halas, T.R. Lee, Preparation and characterization of gold nanoshells coated with self-assembled monolayers, *Langmuir*, 18 (2002) 4915-4920.
- [11] L.R. Hirsch, A.M. Gobin, A.R. Lowery, F. Tam, R.A. Drezek, N. Halas, J.L. West, Metal nanoshells, *Annals of Biomedical Engineering*, 34 (2006) 15-22.
- [12] S. Kalele, S.W. Gosavi, J.S. Urban, K. Kulkarni, Nanoshell particles: synthesis, properties and applications, *Current Science*, 91 (2006) 1038-1052.
- [13] K. Xu, J. Wang, X. Kang, Chen, *J. Mater. Lett.* 63 (2009) 31.
- [14] S. Tang, Y. Tang, S. Zhu, H. Lu, X. Meng, Synthesis and characterization of silica-silver core-shell composite particles with uniform thin silver layers. *J. Solid State Chem.* 180 (2007) 2871-2876.
- [15] M. Zhu, G. Qian, Z. Hong, Z. Wang, X. Fan, M. Wang, Preparation and characterization of silica-silver core-shell structural submicrometer spheres, *J. Phys. Chem. Solids.* 66 (2005) 748-752.
- [16] G. Ding, G. Qian, Z. Wang, J. Qiu, M. Wang, Fabrication and properties of multilayer-coated core-shell structural monodisperse spheres and close-packed structure, *Mater. Lett.* 60 (2006) 3335-3338.
- [17] M. Zhu, G. Qian, G. Ding, Z. Wang, M. Wang, Plasma resonance of silver nanoparticles deposited on the surface of submicron silica spheres, *Mater. Chem. Phys.* 96 (2006) 489-493.
- [18] J.B. Jackson, N.J. Halas, Silver nanoshells: variations in morphologies and optical properties, *J. Phys. Chem. B.* 105 (2001) 2743-2746.
- [19] A. Warshawsky, D.A. Upson, Zerovalent metal polymer composites. I. Metallized beads, *J. Polym. Sci. Part A: Polym. Chem.* 27 (1989) 2963-2994.
- [20] S. Tang, Y. Tang, F. Gao, Z. Liu, X. Meng, Ultrasonic electrodeposition of silver nanoparticles on dielectric silica spheres, *Nanotechnology*, 18 (2007) 295607.
- [21] L. Abbasi, K. Hedayati, D. Ghanbari, Magnetic properties and kinetic roughening study of prepared polyaniline: lead ferrite, cobalt ferrite and nickel ferrite nanocomposites electrodeposited thin films, *J. Mater. Sci: Mater Electron* 32 (2021) 14477-14493.
- [22] Y. Han, J. Jiang, S.S. Lee, J.Y. Ying, Reverse microemulsion-mediated synthesis of silica-coated gold and silver nanoparticles, *Langmuir*, 24 (2008) 5842-5848.
- [23] X. Ye, Y. Zhou, J. Chen, Y. Sun, Deposition of silver nanoparticles on silica spheres via ultrasound irradiation. *Appl. Surf. Sci.* 253 (2007) 6264-6267.
- [24] H. Hofmeistera, P.T. Micleaa, M. Steena, W. Morkeb, H. Drevsc, Structural characteristics of oxide nanosphere supported metal nanoparticles. *Top. Catal.* 46 (2007) 11-21.
- [25] M. Ocana, W.P. Hsu, E. Matijevic, Preparation and properties of uniform-coated colloidal particles. 6. Titania on zinc oxide. *Langmuir*, 7 (1991) 2911-2916.
- [26] S.L. Westcott, S.J. Oldenburg, T.R. Lee, N.J. Halas, Formation and adsorption of clusters of gold nanoparticles onto functionalized silica nanoparticle surfaces, *Langmuir*, 14 (1998) 5396-5401.
- [27] R.D. Badly, W.T. Ford, F.J. MacEnroe, R.A. Assink, Surface modification of colloidal silica, *Langmuir*, 6 (1990) 792-801.
- [28] A. Van Blaaderen, A. Vrij, Synthesis and characterization of monodisperse colloidal organo-silica spheres, *Journal of Colloid and Interface Science*, 156 (1993) 1-18.

- [29] M. Goodarzi, S. Joukar, D. Ghanbari, K. Hedayati, CaFe_2O_4 -ZnO magnetic nanostructures: photo-degradation of toxic azo-dyes under UV irradiation. *J Mater Sci: Mater Electron* 28 (2017) 12823–12838.
- [30] Z. Ebrahimi, K. Hedayati, & Ghanbari. D, Preparation of hard magnetic $\text{BaFe}_{12}\text{O}_{19}$ - TiO_2 nanocomposites: applicable for photo-degradation of toxic pollutants. *J Mater Sci: Mater Electron*, 28 (2017) 13956–13969.
- [31] K. Hedayati, S. Azarakhsh, J. Saffari, D. Ghanbari, Photo catalyst CoFe_2O_4 -CdS nanocomposites for degradation of toxic dyes: investigation of coercivity and magnetization. *J Mater Sci: Mater Electron* 27 (2016) 8758–8770.
- [32] H.B. Ahmed, M.A. Attia, F.M. El-Dars, H.E. Emam, Hydroxyethyl cellulose for spontaneous synthesis of antipathogenic nanostructures:(Ag & Au) nanoparticles versus Ag-Au nano-alloy. *Int. J. Biol. Macromol.* 128 (2019) 214-229.
- [33] H.B. Ahmed, H.E. Emam, Synergistic catalysis of monometallic (Ag, Au, Pd) and bimetallic (AgAu, AuPd) versus Trimetallic (Ag-Au-Pd) nanostructures effloresced via analogical techniques. *J. Mol. Liq.* 287 (2019) 110975.
- [34] Q. Han, C. Zhang, W. Gao, Z. Han, T. Liu, C. Li, Z. Wang, E. He, H. Zheng, Ag-Au alloy nanoparticles: Synthesis and in situ monitoring SERS of plasmonic catalysis. *Sensors Actuators, B Chem.* 231 (2016) 609-614.
- [35] K. Daware, M. Kasture, Kalubarme, R., Shinde, R., Patil, K., Suzuki, N., Terashima, C., Gosavi, S. and Fujishima, A., Detection of toxic metal ions Pb^{2+} in water using $\text{SiO}_2@ \text{Au}$ core-shell nanostructures: A simple technique for water quality monitoring, *Chemical Physics Letters*, Vol. 732 (2019) 136635.
- [36] A.R. Radnaeva, S.V. Kalashnikov, Nomoev, A.V. Nature of diffraction fringes originating in the core of core-shell nanoparticle Cu/SiO_2 and formation mechanism of the structures. *Chemical Physics Letters*, 651 (2016) 274–277.
- [37] K. Manivannan, C.C. Cheng, R., Anbazhagan, Tsai, H.C. and Chen, J.K., Fabrication of silver seeds and nanoparticle on core-shell $\text{Ag}@ \text{SiO}_2$ nanohybrids for combined photothermal therapy and bioimaging. *Journal of Colloid and Interface Science*, 537 (2019) 604–614.
- [38] A. Sakthisabarimoorthi Dhas, S.M.B. and Jose, M. Fabrication and nonlinear optical investigations of $\text{SiO}_2@ \text{Ag}$ core-shell nanoparticles, *Materials Science in Semiconductor Processing*, 71 (2017) 69–75.